Epitaxial thin-film growth of C_{60} on VSe_2 studied with scanning tunneling microscopy and x-ray diffraction

R. Schwedhelm, J.-P. Schlomka, S. Woedtke, R. Adelung, L. Kipp,* M. Tolan, W. Press, and M. Skibowski
Institut für Experimentelle und Angewandte Physik, Universität Kiel, D-24118 Kiel, Germany
(Received 23 July 1998; revised manuscript received 1 December 1998)

The growth of C_{60} films on layered 1T-VSe_2 has been investigated by combined scanning tunneling microscopy (STM) and x-ray diffraction. The STM results are discussed in the framework of the diffusion limited aggregation (DLA) model. Particularly, the crossover from fractal to uniform growth as a function of the aggregated particle concentration is studied and discussed in the context of DLA. The averaged vertical structure is determined by Bragg diffraction and x-ray reflectivity and is explained in conjunction with the STM results. The epitaxial growth in the (111) direction is confirmed and a homogeneous layer thickness is found. Interfacial roughness and the averaged dispersion of the film are derived from the data.
[S0163-1829(99)10019-5]

I. INTRODUCTION

Since the discovery of C_{60} (Ref. 1) and the breakthrough in the synthesis of macroscopic quantities[2] the physical properties of this third allotropic form of carbon have been widely studied. As shown in a previous study,[3] the electronic structure of C_{60} films grown on various substrates is strongly affected by the interaction between the substrate and the sublimed film. Furthermore, it was proved that VSe_2 is an ideal substrate for C_{60} in view of measuring the intrinsic electronic properties of fullerenes. Therefore, it is desirable to investigate the undistorted growth of C_{60} on VSe_2. Scanning tunneling microscopy (STM) is an efficient tool to study the nucleation of C_{60} and the growth of thin C_{60} films on an atomic scale. Also, information about the substrate-adsorbate interaction can be obtained. In previous studies fullerene films were characterized on different substrates such as various semiconductor surfaces,[4–10] metals,[11–18] and layered materials.[19,20] A common result for deposition on semiconductors is the strong bonding of the fullerenes due to the interaction between the dangling bond states of the semiconductor surfaces and the empty C_{60} orbitals. Therefore, either the deposited fullerenes were orderless or several distinct island orientations were found. Smalley and co-workers[21] have found distinct mixed domains with compressed nearest neighbor distance of C_{60} on GaAs (110). Xue *et al.*[22] pointed out that the interaction between C_{60} molecules and the GaAs (001) surface extends up to the third monolayer, leading to irregular structures of molecular disorder. Even rearrangements of the topmost substrate atoms after fullerene adsorption are reported.[5] In the case of metallic substrates also a strong chemisorption of C_{60} via charge transfer takes place, leading to stressed fullerene layers and to adsorbate induced reconstruction of the substrate.

Layered materials should be very suitable for the epitaxial accommodation of C_{60} because they exhibit rather small van der Waals forces at the surface and in general show a low density of defects. Schwarz *et al.*[19] found that epitaxial growth of C_{60} on GeS (001) only takes place in a small range of elevated substrate temperatures. This indicates a limited surface mobility of the C_{60} molecules at room temperature, probably due to the corrugated substrate surface. Unfortunately this study was performed in air and the authors found indications of oxidation effects. Zhao, Chen, and Wang pointed out[20] that the coupling between the (0001) surface of the layered material MoS_2 and single fullerene molecules is weak and that no charge transfer or chemical bond formation occurs. This work deals with electronic correlation effects between single C_{60} molecules and the substrate but the growth nature was not investigated.

It is the aim of the present paper to discuss the growth mechanism of C_{60} on VSe_2. A single crystal of layered VSe_2 was chosen as a substrate for deposition of C_{60} in view of a suitable lattice constant and weak interaction with the adsorbate. The lattice constant $a = 3.35$ Å (see Ref. 23) of its hexagonal (0001) surface matches to one-third of the nearest neighbor distance of the (111) surface in a fcc C_{60} crystal, which is 10.02 Å.[2] Because of the negligible interaction between the substrate surface and the C_{60} molecules together with the absence of lattice mismatch the ideal assumptions of the diffusion limited aggregation (DLA) model developed by Witten and co-workers[24,25] are fullfilled. Therefore the growth mechanism is discussed in this framework and special effort is made to explain the crossover from fractal to uniform growth.

In order to gain information not only about the topmost C_{60} layers accessible with STM but also to understand the vertical composition of multiple film growth we applied x-ray reflectometry. This, in particular, is an efficient tool to study structural properties, e.g., film thicknesses, electron densities, and interface roughnesses.[26–28] In combination with conventional Bragg scattering a rather accurate picture of the sample structure on microscopic and mesoscopic length scales is obtained. In contrast to direct methods such as STM the information cannot be extracted from the measurements directly. Instead, in most cases the structure has to be modeled and the simulated scattering of the model system is compared with the measurement. Thus investigations with both direct and indirect methods increase the plausibility of the assumed model. On the other hand, using x-rays of well-

defined energy, absolute length scales of the system can be measured with high accuracy. Vertical length scales (e.g., film thicknesses) are most easily obtainable. This is a useful complement to STM which gives accurate information about lateral structures. STM pictures only depict a tiny region (typically 1 μm^2) of the sample, whereas x-ray scattering averages over a macroscopic sample region (typically 1 mm^2). The combination of these two techniques gives a rather complete description of the sample morphology.

II. SAMPLE PREPARATION AND EXPERIMENTAL SETUP

The crystal structure of the VSe_2 substrate consists of two-dimensional Se-V-Se sandwiches in 1T coordination[23] separated by a van der Waals gap. The material can easily be cleaved along this gap, producing well-ordered surfaces which exhibit extremely low defect densities. C_{60} molecules[29] were evaporated onto cleaved VSe_2 from a temperature controlled effusion cell at 565 K. The substrate temperature during fullerene evaporation was tunable from room temperature up to 800 K via a resistive heating unit mounted on the sample holder. During the preparation the total pressure in the molecular beam epitaxy (MBE) chamber was in the lower 10^{-10} mbar range monitored by a mass spectrometer. The thickness of the deposited material was estimated via STM. For various temperatures and evaporation times the fullerene deposition on clean substrates was measured, so that parameters for single monolayer preparation could be derived.

The STM (Ref. 30) used for the topographic measurements consists of a single-tube scanner system mounted on a vibration damping with an eddy current attenuation. The tips were produced by etching tungsten wire and are changeable by transfer in the ultrahigh vacuum (UHV) system. Via this transfer system the STM is connected to the preparation chamber. Therefore the prepared samples were investigated without breaking the UHV. For calibration of the length scales silicon single crystals were used. The C_{60} coverage of the scanned areas can be determined within $\pm 1\%$. Positive bias voltage corresponds to electrons tunneling in empty states of the sample. STM images were taken at room temperature in the constant current mode. I_T denotes the tunneling current.

The x-ray experiments were performed using a 12 kW rotating anode source with Cu target ($\lambda = 1.54$ Å, size of the beam spot on the sample 0.3×1 mm^2) and a two-circle diffractometer as described in Ref. 31. A reflectivity scan is performed by rotating the sample and the detector in a manner such that the angle of incidence α_i equals the exit angle α_f. The scattering angle Φ is given by $\Phi = \alpha_i + \alpha_f$. Thus for a reflectivity scan $\alpha_i = \Phi/2$ is fulfilled. This results in a wave vector transfer $\vec{q} = (0,0,q_z)^T$ perpendicular to the surface where q_z is given by $q_z = (4\pi/\lambda)\sin(\alpha_i)$. Consequently the sample structure in z direction (film thickness, roughnesses, etc.) is probed. A rocking scan (or ω scan) is performed by placing the detector at a fixed angle Φ and rotation of the sample.

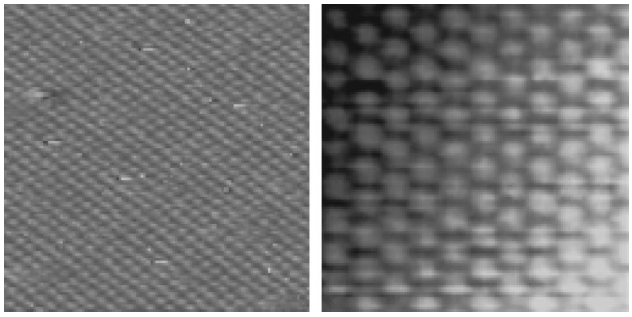

FIG. 1. STM image of unoccupied states of the clean VSe_2 substrate (left) and the C_{60} overlayer (right) deposited at 293 K substrate temperature. Bias is +2 V, $I_T = 0.5$ nA, and the depicted area amounts to 9×9 nm^2.

III. RESULTS AND DISCUSSION

Figure 1 shows a STM image of empty states of the clean VSe_2 substrate (left part) together with a part of the first monolayer of C_{60} adsorbed at 293 K substrate temperature (right part). The depicted area of both images amounts to 9×9 nm^2. The substrate is almost perfectly flat and the absence of defects and kink sites favors the epitaxial aggregation of C_{60} molecules. The lattice parameter of $1T-VSe_2$ amounts to 3.4 Å, in agreement with Ref. 23. In the right panel we show the result after adsorption of fullerenes of the first monolayer on the same length scale. Neither defects nor steps are visible and the hexagonal arrangement of the single molecules can be observed. This epitaxial (111) overlayer of fullerenes exhibits a nearest neighbor distance of 10.3 Å in accordance with Ref. 2.

It is easily calculated that an area of 1000×1000 nm^2 contains 1.15×10^6 hexagonal close packed fullerene molecules which is defined as one monolayer. Figure 2 shows a STM topograph of C_{60} grown on VSe_2 at room temperature. The substrate appears to be perfectly flat. In the first monolayer we observe roundish islands of C_{60} (about 400 nm diameter) covering 59% of the surface. On the top of these islands (in the second layer) small fractal shaped islands (up to 100 nm diameter) are evident. By using a topographic profile (see lower part of Fig. 2) the roundish islands are identified as the first monolayer about 9 Å above the substrate while the second layer is represented by small fractal islands. The step height between the first and the second layer of fullerenes amounts to 8 Å, which corresponds nearly perfectly to the theoretical spacing of 8.2 Å between (111) planes in a C_{60} fcc lattice with 10.02 Å nearest neighbor distance. Between the islands of the first layer the bare substrate is discernible (see Fig. 1) which amounts to 41% of the scanned area. The first steps of epitaxial growth of C_{60} on VSe_2 can be described in the context of the diffusion limited aggregation model. A simulation of this model was performed by Witten and Sander.[24] Initially, lattice points of the substrate are occupied by some seed particles. Each deposited particle is placed on a random lattice point and then is allowed to diffuse randomly on the surface until it reaches a lattice position adjacent to an occupied site. There the particle sticks and the procedure is iterated with the next particle.

As the molecular flux during the C_{60} preparation is very low (0.05 monolayers per minute) and the interaction be-

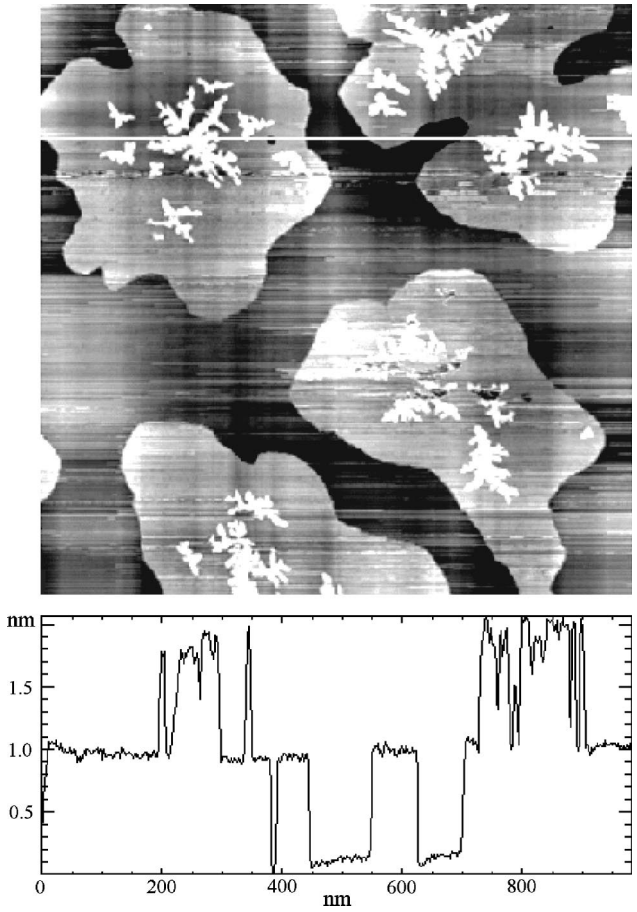

FIG. 2. STM picture of occupied states of VSe_2 that is covered with C_{60} at room temperature. Lateral dimension is 1000×1000 nm^2. The roundish islands are composed of fullerene molecules of the first monolayer. Before completion of the first monolayer the growth of the second monolayer starts which shows small fractal islands. The coverage of the first monolayer of C_{60} amounts to 59% and the second monolayer to 7%. The bias was -2.5 V and the tunneling current 0.4 nA. At the bottom a topographic profile along the white line of the STM image is depicted.

tween the substrate and the adsorbate as well as the interaction between two fullerene layers is rather small (van der Waals type) the conditions for undistorted diffusion of single C_{60} molecules are fulfilled. Applying this model we can explain the different shapes of the islands of the first and second monolayer. According to Ref. 25 the diffusion length ξ is given as

$$\xi^2 = c^{-1} R^{D-d+2}. \tag{1}$$

R is the averaged cluster radius in units of lattice points which are separated by the nearest neighbor distance of C_{60} molecules. c is the surface concentration of occupied lattice points, d is the dimension of the simulation ($d=2$), and $D = \frac{5}{3}$ represents the Hausdorff dimension which is independent of the chosen lattice.[25] The transition from fractal to nonfractal growth takes place if

$$R_{\mathrm{crit}} := R = \xi,$$

where R_{crit} stands for the critical radius. Hence, with Eq. (1) follows

$$R_{\mathrm{crit}}^{D-d} = c_{\mathrm{crit}}. \tag{2}$$

If $\overline{R}$ denotes the average distance of the seed particles the point of transition is reached for $R_{\mathrm{crit}} = \overline{R}$. With c_0 describing the concentration of the seed clusters it follows that (for more details see Ref. 25)

$$\overline{R} = c_0^{-1/d}. \tag{3}$$

Figure 2 shows four seed clusters in the first monolayer. Therefore $c_0 = (4/1.15) \times 10^{-6}$ and Eq. (3) yields $\overline{R} = 540$ lattice distances. With Eq. (2) we conclude $c_{\mathrm{crit}} = 12\%$. The measured concentration is 59%, much higher than the critical concentration. Hence, the islands of the first monolayer are not fractal. Let us consider the second monolayer now. Since 59% of the total area is covered with the first monolayer of C_{60} the base of the second monolayer consists of 6.79×10^5 fullerene molecules. With 25 tiny clusters of the second layer we find analogously $R_c = 165$ lattice distances. Thus the critical concentration is found to be $c_{\mathrm{crit}} = 18\%$. This value is significantly higher than the measured second monolayer coverage (relative to the first monolayer) of 12%. It follows that the shape of the islands of the second layer is fractal. In DLA the exposed ends of the clusters grow more rapidly than the interior, because the random walkers are captured before they reach the interior. This explains why the incoming particle flux is screened by the cluster itself. If the critical concentration of particles at the surface is not exceeded one would expect larger branches of fractal aggregations. Thus larger islands of the second monolayer in Fig. 2 located in the middle of the underlying first monolayer represent early stages of aggregation while the surrounding smaller ones are later.

In order to derive some margin of error for the critical coverages in the first and the second C_{60} monolayer the calculation based on Fig. 2 was repeated for several sample areas. After the consideration of the first C_{60} layer had revealed an uncertainty of only $\pm 1\%$ for the transition concentration, the critical coverage in the following monolayer was found to be strongly influenced by the local seed cluster geometry. Here a statistical variation up to $\pm 5\%$ was obtained. Regardless of these estimations the nonfractal islands always clearly exceeded the critical values, while the concentration of the fractal-like toplayer islands was always just below the critical percentage.

Because of the small interaction between the substrate and the adsorbate fractal islands should also be visible in the first monolayer and the question arises of where the crossover from fractal to uniform growth takes place. To study this topic a sample with a lower coverage of fullerenes was prepared at room temperature. Compared to Fig. 2 no seed clusters of the second monolayer are visible. A STM image illustrating the fractal history of an island of the first monolayer is depicted in Fig. 3. The former fractal branches are already round due to further aggregation of fullerenes. The critical concentration is just exceeded. It is noteworthy that the interaction between the STM tip and the fullerenes of smaller islands is stronger than the substrate-adsorbate interaction, resulting in the deformation of the islands during the scanning process. Although the cohesive energy in bulk fcc C_{60} amounts to 1.6 eV,[32] it is likely that the molecules of

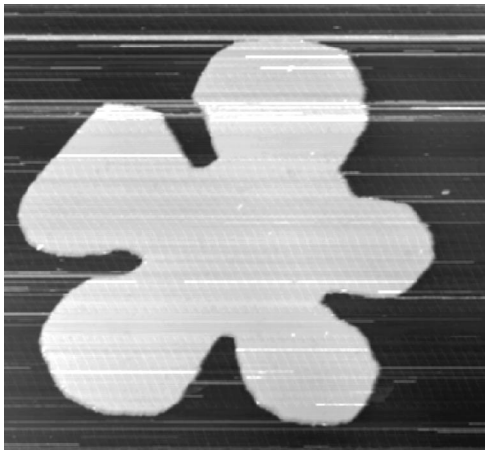

FIG. 3. Empty state STM image of the first monolayer of C_{60} grown at room temperature (bias is $+1.59$ V, $I_S=0.11$ nA). The lateral dimension is 500×500 nm^2. Crossover from fractal to uniform growth has already taken place but the fractal history of this island is still discernible.

the first monolayer exhibit a significant lower cohesive energy because of the lower coordination with other molecules.

To further corroborate the application of the DLA model to fullerenes condensed onto VSe_2 the substrate temperature during the preparation was increased from room temperature to 340 K (see Fig. 4). In general this leads to a decrease of the sticking coefficient. Because at small distances (the length scale of a fractal cluster) the concentration of aggregating particles is found to be roughly constant[24] it is predicted that a smaller sticking coefficient results in a broadening of the fractal branches. Beyond the critical concentration the uniform islands are expected to be rounded. This is actually what can be observed in the experiment. In comparison to Fig. 2 the branches of the fractal islands are thicker and the islands of the first monolayer are rounded according to the predictions of the DLA model. Furthermore, the number of fractal islands of the second monolayer is much lower than in Fig. 2 even though the overall coverage with fullerenes is almost the same. This can be explained in terms of the increased mobility of the incoming molecules due to the elevated substrate temperature which enables the particles to move towards the island edges to be

FIG. 4. STM empty states picture of a 58% coverage of C_{60} on VSe_2 prepared at 340 K scanned with a bias of $+2$ V and $I_T=1$ nA. The lateral dimension is 1000×650 nm^2.

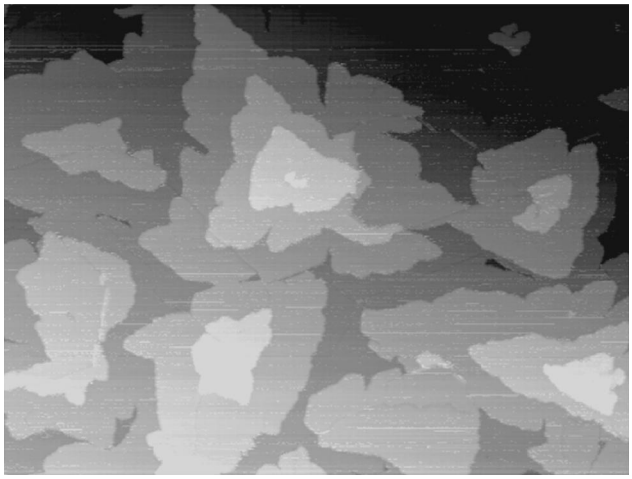

FIG. 5. STM empty states image of a thick C_{60} film grown at 340 K recorded with a bias of $+2.2$ V and a tunneling current of 0.2 nA. The lateral dimension is 1000×820 nm^2. Up to five incomplete monolayers of C_{60} are visible. In comparison with Fig. 2 the topmost layer is not fractal, in line with DLA predictions.

aggregated there. It is noteworthy that desorption of the fullerenes starts for substrate temperatures higher than 470 K. The comparison with the evaporation temperature of 565 K (see Sec. II) indicates that the substrate-fullerene bonding is smaller than the weak van der Waals bonding between C_{60} molecules. To study the later stage of C_{60} growth a thicker film was deposited at room temperature. Figure 5 shows a STM image of this film where up to five incomplete monolayers of C_{60} are visible. The low lying islands have grown towards each other. But the coalescence is not perfect and tiny holes in this monolayer remain. We want to outline why the topmost layer in Fig. 5 does not show fractal growth. The topmost layer covers 31% of the next monolayer. An analogous calculation as above yields a critical concentration of 18%. According to DLA the actual coverage is larger than the crossover coverage and thus the growth is already uniform.

The lateral structure of the top layers of C_{60} on VSe_2 can be adequately studied using STM. However, the buried structure perpendicular to the surface down to the substrate-fullerene interface has to be investigated by different means. Here we apply conventional x-ray reflectometry and Bragg diffraction. Yet, the experiment is complicated by the fact that in comparison to the perfect substrate lattice on small length scales (Fig. 1) the surface possesses waviness on a macroscopic scale. Therefore a narrow specular reflection occurs in a rocking scan whenever a flat part of the surface fulfills the condition $\alpha_i=\alpha_f$. Two additional specular peaks beside the twinned main peak can be seen in Fig. 6(a) where a scan at $q_z=0.028\,\text{Å}^{-1}$ is shown. The most intense peak was picked for the reflectivity measurement. In principle the integral over all specular peaks has to be taken as the total reflected intensity. However, since the full width at half maximum (FWHM) of the most intense peak remains constant over the whole q_z range, the reflectivity can be correctly recorded by just measuring the intensity of this peak. To obtain the ''true specular reflectivity'' a background has to be subtracted from the measured reflectivity. This is done by carrying out a so-called longitudinal diffuse scan. Such a

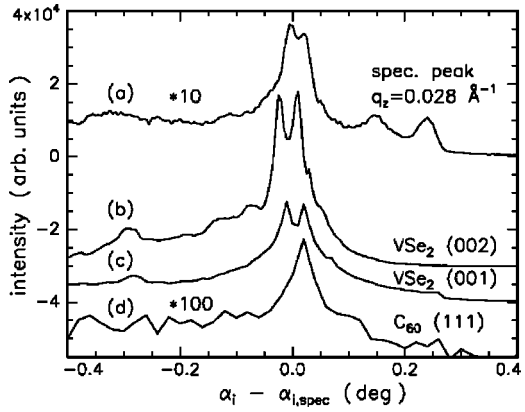

FIG. 6. Rocking curves through (a) the specular ridge at $q_z = 0.028$ Å^{-1}, (b) the VSe_2 (001), (c) the VSe_2 (002), and (d) the C_{60} (111) peak. A twinned maximum with a tilting angle of 0.03° can be seen for the specular reflection and the substrate peaks. This is caused by two single crystalline domains in the substrate. The scans are shifted on the intensity scale for clarity.

scan is performed by rotating the sample and the detector fulfilling $\alpha_i = \Phi/2 + \Delta\alpha_i$, where $\Delta\alpha_i$ is a fixed offset angle. Figure 7 shows the true reflectivity of the thick C_{60} film.[33] Since the real part of the refractive index $n = 1 - \delta + i\beta$ (δ dispersion, β absorption, $\delta, \beta \sim 10^{-6}$) is slightly smaller than unity, total external reflection occurs for incident angles $\alpha_i < \alpha_c$, where $\alpha_c \simeq \sqrt{2\delta}$. The dispersion δ is proportional to the electron density, and therefore from the critical angle of a known material the mass density can be calculated. For very thin films (<200 Å) the critical angle is given by the underlying substrate material, here VSe_2 ($\alpha_c = 0.32°$). For incident angles larger than α_c the reflectivity decreases rapidly, showing oscillations caused by the interference of beams reflected at the C_{60}/air and the VSe_2/C_{60} interfaces, respectively. The oscillation period is inversely proportional to the thickness of the film whereas the decay is influenced by the roughness of the substrate and the film. A quantitative analysis was done by calculating the reflectivity of a film-substrate system using the well-known Parratt algorithm[26,28] and adjusting the film thickness, the electron density, and the profile of the two interfaces. Without any *a priori* knowledge of the sample a fit with a single layer of C_{60} on VSe_2 was performed. The film thickness was found to be $d = (46 \pm 3)$ Å, with roughnesses of $\sigma_1 < 2.5$ Å for the substrate/film interface and $\sigma_2 = (5 \pm 3)$ Å for the C_{60}/air interface. The small roughnesses prove that the total film thickness does not vary significantly over a large sample area. From the fit with the single-layer model one obtains the dispersion $\delta = (4.8 \pm 0.7) \times 10^{-6}$. Calculating the dispersion for a single crystal of C_{60} with a lattice parameter of 14.17 Å (Refs. 34 and 35) yields the larger value $\delta = 5.4 \times 10^{-6}$. However, a value of 4.5×10^{-6} was found for spin cast C_{60} on glass also determined by x-ray reflectivity.[36] In our case we obtain from simulations using different densities for the film that this parameter mainly influences the decay above the critical edge and the height of the first oscillation. Since we measured only the reflectivity on top of the most intense peak of a rocking curve (see above) and hence the reflectivity below the critical edge was only 25% of the primary beam intensity, the height of the total reflectivity plateau may not be accurately determined. This results in the large error bar for the dispersion of the film as given above. Since the STM revealed a coverage $\geqslant 96\%$ the dispersion calculated from the bulk density of C_{60} was used in the simulations shown in Fig. 7.

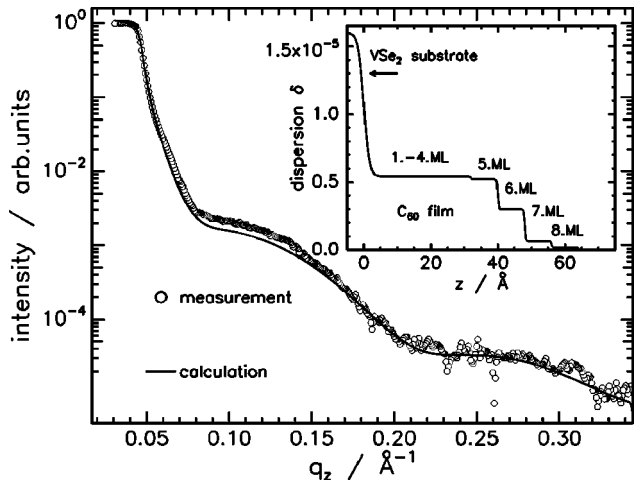

FIG. 7. Measurement (symbols) and model calculations (lines) of the true specular reflectivity of the thick C_{60} film. Model 1 (solid line) assumes a simple one-layer system on the substrate. Model 2 (dashed line) assumes the monolayer coverage obtained by STM. The models are explained in the text. The inset shows the dispersion ($\propto$ electron density) depth profiles used for the model calculation.

To compare the x-ray results with the surface structure measured by STM (Fig. 5) the coverages of the four topmost C_{60} monolayers were extracted from the image, revealing 96%, 55%, 12%, and 3%, respectively. With these data a density profile was modeled assuming steps between the monolayers (inset of Fig. 7). Such a density was then used to calculate the reflectivity. The only adjustable parameters were the thickness of the underlying complete C_{60} monolayers and the roughness of the VSe_2/C_{60} interface. It turned out that this profile can indeed explain the reflectivity data. The thickness of the underlying completed monolayers was 32 Å, which corresponds to four C_{60} monolayers. By varying the monolayer coverage in the refinement the sensitivity on the fit was tested. Values of $(90 \pm 10)\%$ for the fifth ML, $(50 \pm 15)\%$ for the sixth ML, $(12 \pm 8)\%$ for the seventh ML, and $\leqslant 10\%$ for the eighth ML were found. This shows that the fit is sensitive to the C_{60} coverage. Furthermore, the x-ray results confirm that the local composition of the sample as determined by STM is present over a much larger area (illuminated area approximately 1 mm^2).

To investigate the atomic spacing of the C_{60} monolayers perpendicular to the surface an $\alpha_i - 2\alpha_i$ scan in the wide-angle region (wide-angle reflectivity) was carried out. This type of scan is sensitive to the *c* lattice parameter of the hexagonal VSe_2 unit cell and the (111) lattice spacing of the C_{60} film. Figure 8 shows the resolution limited Bragg peak of the substrate and the weak broad peak caused by the C_{60} overlayer. From the analysis of the data the *c* lattice parameter of the substrate was found to be (6.10 ± 0.01) Å, which is in very good agreement with literature values.[37,23] A simple analysis using a single Laue function $I \sim \sin^2(Naq_z/2)/\sin^2(aq_z/2)$ would yield a lattice parameter of $c_{111} = (8 \pm 0.4)$ Å for the C_{60} lattice spacing. This corre-

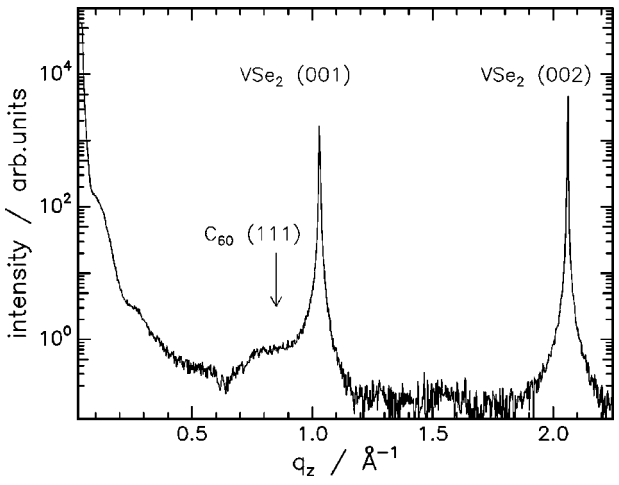

FIG. 8. Bragg scan ($\Theta-2\Theta$ scan) of the C_{60} sample with more than four complete monolayers. The intense peaks are the (001) and (002) substrate reflections. Their positions (14.52° and 29.26°) correspond to a lattice spacing of 6.10 Å. The broad feature at $q_z = 0.85$ Å^{-1} is the (111) C_{60} peak.

sponds to a fcc lattice parameter of $a \sim 13$ Å which differs significantly from the bulk value of $a = 14.17$ Å. Furthermore, we obtain $N = (4 \pm 1)$ as the number of coherently scattering C_{60} layers. While the value of N can be determined rather accurately this does not hold for the lattice spacing a because of the strong scattering from the substrate. A sophisticated analysis based on a complete calculation of the scattering using the Born approximation for layer systems[38] reveals that a may vary between 12.8 Å and 14.4 Å depending on particular model assumptions. However, the weak scattering from the few C_{60} monolayers renders a further analysis virtually impossible.

The obtained number of coherently scattering C_{60} planes and the small substrate/film roughness shows that the epitaxy of the films is of good quality. Rocking scans through the substrate reflections show a broadened peak caused by two single-crystal domains tilted by an angle of 0.03° [Figs. 6(b) and 6(c)]. This can also be seen in the transverse scan obtained in the low-angle regime [Fig. 6(a)]. However, the splitting cannot be observed in the transverse scan through the C_{60}(111) peak [Fig. 6(d)], indicating that the C_{60} growth was not influenced by this specific substrate property.

Table I summarizes the film parameters resulting from the x-ray analysis.

TABLE I. Results of the refinement of the x-ray measurements on the thick C_{60} film. Dispersions δ, roughnesses σ, and thickness d result from the refinement of the reflectivity. The lattice spacings in q_z direction and the number N of coherently scattering atomic layers are extracted from the $\alpha_i - 2\alpha_i$ scan.

	Substrate	C_{60} layer
Dispersion $\delta \times 10^6$	16.0 ± 0.3	4.8 ± 0.7
Roughness σ / Å	$\leqslant 2.5$	5 ± 3
Thickness d / Å		46 ± 3
Lattice spacing c / Å	6.10 ± 0.01	7.4-8.3
Number of layers N	>170	4 ± 1

IV. SUMMARY AND CONCLUSIONS

We have studied the growth of C_{60} films on the layered material VSe_2 at room temperature and 340 K using two complementary methods, STM and x-ray diffraction. The major findings of our study follow. (i) Due to its special structure the VSe_2 substrate allows an undistorted epitaxial growth of C_{60} layers which leads to fractal cluster shapes for low coverages at room temperature and roundish islands for higher coverages and/or temperatures. (ii) The two different growth modes and the transition concentrations are well described within the diffusion limited aggregation model. Thus, the C_{60}/VSe_2 interface is an almost perfect physical realization of DLA and allows a quantitative comparison of the theory with experimental data. (iii) Additional x-ray scattering measurements in the total external reflection regime revealed that the STM shows a representative image of the sample surface. Furthermore, the very small interface roughness proved the almost perfect epitaxial growth of the C_{60} layers. (iv) For additional growth characterization wide-angle Bragg scattering studies were performed. Four completed C_{60} monolayers in (111) orientation were observed, indicating a homogeneous high quality sample.

This demonstrates the consistence of the results obtained by complementary structural techniques which probe extremely different length scales. In future, it will be possible to investigate directly the atomic arrangements of the islands with microfocus beams which are available at third generation synchrotron x-ray sources such as ESRF and APS. Thus the structure of single islands may be accessible rather than an average picture which was obtained in our study.

ACKNOWLEDGMENTS

This work was supported by BMBF, FR Germany (Project Nos. 05 605 FKB and 05 SB8 FKB). The support of J.-P.S. by the Volkswagenstiftung (Project No. I/71128) is gratefully acknowledged.

*Author to whom correspondence should be addressed.

[1] H.W. Kroto, J. H. Heath, S.C. O'Brian, R. F. Curl, and R. E. Smalley, Letters to Nature **318**, 162 (1985).

[2] W. Krätschmer, L.D. Lamb, K. Fostiropoulos, and D.R. Huffmann, Nature (London) **347**, 355 (1990).

[3] R. Schwedhelm, L. Kipp, A. Dallmeyer, and M. Skibowski, Phys. Rev. B **58**, 13 176 (1998).

[4] X.D. Wang, T. Hashizume, and T. Sakurai, Mod. Phys. Lett. B **8**, 1597 (1994).

[5] K.R. Wirth and J. Zegenhagen, Phys. Rev. B **56**, 9864 (1997).

[6] Y.-R. Ma, P. Moriarty, and P.H. Beton, Phys. Rev. Lett. **78**, 2588 (1997).
[7] A.W. Dunn, P. Moriarty, M.D. Upward, and P.H. Beton, Appl. Phys. Lett. **69**, 506 (1996).
[8] X. Yao, T. G. Ruskell, R. K. Workman, D. David, and D. Chen, Surf. Sci. **366**, L743 (1996).
[9] H. Xu, D.M. Chen, and W.N. Creager, Phys. Rev. Lett. **70**, 1850 (1993).
[10] Q. Xue, Y. Ling, T. Ogino, T. Sakata, Y. Hasegawa, T. Hashizume, H. Shinohara, and T. Sakurai, Thin Solid Films **281-282**, 618 (1996).
[11] Y. Maruyama, K. Ohno, and Y. Kawazoe, Phys. Rev. B **52**, 2070 (1995).
[12] M.K.-J. Johansson, A. J. Maxwell, S. M. Gray, P. A. Brüwiler, D. G. Mancini, L. S. O. Johansson, and N. Mårtensson, Phys. Rev. B **54**, 13 472 (1996).
[13] B. Reihl, in *Science and Technology of Fullerene Materials*, edited by P. Bernier, T.W. Ebbesen, D.S. Bethune, R. M. Metzger, L.Y. Chiang, and J.W. Mintmire, MRS Symposia Proceedings No. 359 (Materials Research Society, Pittsburgh, 1995), p. 379.
[14] T. David, J. K. Gimzewski, D. Purdie, B. Reihl, and R. R. Schlitter, Phys. Rev. B **50**, 5810 (1994).
[15] J.K. Gimzewski, S. Modesti, and R.R. Schlittler, Phys. Rev. Lett. **72**, 1036 (1994).
[16] Y. Kuk, D. K. Kim, Y. D. Suh, K. H. Park, H. P. Noh, S. J. Oh, and S. K. Kim, Phys. Rev. Lett. **70**, 1948 (1993).
[17] T. Michely, M. Hohage, M. Bott, and G. Comsa, Phys. Rev. Lett. **70**, 3943 (1993).
[18] P.W. Murray, M. Ø. Pedersen, E. Lœgsgaard, I. Stensgaard, and F. Besenbacher, Phys. Rev. B **55**, 9360 (1997).
[19] U.D. Schwarz, W. Allers, G. Gensterblum, J.-J. Pireaux, and R. Wiesendanger, Phys. Rev. B **52**, 5967 (1995).
[20] D. Zhao, T. Chen, and L. Wang, Appl. Phys. Lett. **66**, 3292 (1995).
[21] Y.Z. Li, J.C. Patrin, M. Chander, J.H. Weaver, L.P.F. Chibante, and R.E. Smalley, Science **252**, 547 (1991).
[22] Q. Xue, Y. Ling, T. Ogino, T. Sakata, Y. Hasegawa, T. Hashizume, H. Shinohara, and T. Sakurai, Thin Solid Films **281-282**, 618 (1996).
[23] P. H. Dederichs, H. Schober, and D. Sellmeyer, in *Phononenzustände, Elektronenzustände und Fermiflächen*, edited by K.-H. Hellwege and J. L. Olsen, Landolt-Börnstein, New Series, Group III, Vol. 13, Pt. a (Springer-Verlag, Berlin, 1981).
[24] T.A. Witten and L.M. Sander, Phys. Rev. B **27**, 5686 (1983).
[25] T.A. Witten, Jr. and P. Meakin, Phys. Rev. B **28**, 5632 (1983).
[26] L.G. Parratt, Phys. Rev. **95**, 359 (1954).
[27] J. Lekner, *Theory of Reflection* (Martinus Nijhoff Publishers, Dordrecht, 1987).
[28] J.-P. Schlomka, M. Tolan, L. Schwalowsky, O. H. Seeck, J. Stettner, and W. Press, Phys. Rev. B **51**, 2311 (1995).
[29] C_{60} powder obtained from Hoechst AG, Germany; purity 99.78%; C_{70} content of 0.2 ppm.
[30] Micro-STM from Omicron, Taunusstein, Germany.
[31] L. Brügemann, R. Bloch, W. Press, and M. Tolan, Acta Crystallogr., Sect. A: Found. Crystallogr. **A48**, 688 (1992).
[32] S. Saito and A. Oshiyama, Phys. Rev. Lett. **66**, 2637 (1991).
[33] The count rate was corrected by a geometry factor $f = \sin(\alpha_g)/\sin(\alpha_i)$ for $\alpha_i < \alpha_g$ which takes into account that at very small angles not all incoming radiation impinges onto the surface. α_g is the ''angle of full illumination'' given by $\sin(\alpha_g) = b/l$ with b the beam width and l the sample size.
[34] Y. Yoneda, K. Sakaue, and H. Terauchi, J. Phys. Soc. Jpn. **63**, 3560 (1994).
[35] L. Akselrod, H.J. Byrne, T.E. Sutto, and S. Roth, Chem. Phys. Lett. **233**, 436 (1995).
[36] I. Belaish, I. Entin, R. Goffer, D. Davidov, H. Selig, J. P. McCauley, N. Coustel, J. E. Fischer, and A. B. Smith, J. Appl. Phys. **71**, 5248 (1992).
[37] J. Hoschek and K. Klemm, Z. Anorg. Allg. Chem. **242**, 49 (1939).
[38] V. Holý, U. Pietsch, and T. Baumbach, in *X-Ray Scattering from Thin Films*, Springer Tracts in Modern Physics Vol. 149 (Springer, Berlin, 1998).